The 2009 IEEE/RSJ International Conference on
Intelligent Robots and Systems
October 11-15, 2009 St. Louis, USA

Modeling Global Deformation using Circular Beams for Haptic Interaction

Tong Cui, *Member, IEEE*, Jing Xiao, *Senior Member, IEEE*, Aiguo Song, *Member, IEEE*

Abstract—**In this paper, a new method to model the global deformation between a rigid object and an elastic object with a hole is presented. This method extends the idea of beam-skeletons [10] by introducing curved cantilever beams for efficient modeling of global deformation of elastic objects with holes. The method is implemented and tested on different examples. Results from three examples are given to demonstrate the efficiency and effectiveness of the approach.**

I. Introduction

Many applications of haptic interaction involve handling of deformable objects, such as virtual training in surgery operations, interactive computer games, planning of grasping in robotics, tele-robotic operations, etc. Deformable objects in contact have been studied for both graphics rendering and haptic rendering [1] [2] [3].

One major challenge for haptic rendering of contacts involving deformable objects is to balance the requirement of rendering speed for interactive operations and the realism of rendering. To achieve a high rendering rate, existing approaches often apply certain simplifications to the physically based deformable models used in graphics rendering, such as the mass-spring-damper models and continuum models, and focus on simple contact cases [4-7]. The Radial Elements Method (REM) [8] reduces the number of the computed elements to be fast and scalable in simulation of deformations. However, the object shapes that can be modeled are restricted to star-shaped ones (thus without holes). Point-Sampled Thin Shell [9] is an efficient method for simulating deformation of thin shells. This method supports both elastic and plastic deformations as well as fracturing and tearing of the material.

Recently, Luo and Xiao introduced a novel and efficient method for force and deformation modeling between a rigid object and a convex elastic object in interactive environments [10]. The approach is characterized by modeling nonlinear contact forces based on the Duffing equations and simulating global shape deformation by a "beam-skeleton" model based on the beam bending theory. The method has an update rate of several tens of kHz regardless of the object's concrete geometry, which is extremely efficient.

However, deformable objects may also have holes and thus not convex. In this paper, we model global shape deformation (during haptic interaction) of an elastic object with a convex outer shape but with a hole inside. We extend the beam-skeleton model introduced in [10] to include curved cantilever beams for simulating the deformation of such elastic objects. Equations about curved beams based on the elastic theory can be used to relate contact force and deformation nicely.

The paper is organized as follows: In Section II, we review the beam skeleton model introduced in [10]. In Section III, we introduce force analysis based on curved beam theory and describe shape deformation modeling. In Section VI, we discuss implementation and experimental results, and we conclude the paper in Section V.

II. Review of the Beam-Skeleton Model

In [10], a beam-skeleton model with anchor points was introduced to simulate global shape deformation of a convex elastic object under contact from a rigid object. An anchor point is an extremal point on the original (undeformed) surface of the elastic object, capturing the geometric characteristics of the surface [10]. When the elastic object is under contact, the deformation displacements at these anchor points are computed via the beam-skeleton model and then interpolated over the entire surface of the elastic object to simulate global shape deformation.

A. Basic Assumptions on Objects and Contacts

Contacts are considered between a rigid object and an elastic object in a virtual environment. Both objects have triangle mesh models. The elastic object is convex and has smooth surface patches. The interaction between the rigid object and the elastic object is sufficiently slow so that contact forces are caused by quasi-static collisions, and shape deformation of the elastic object only occurs at stable equilibrium configurations, where the elastic energy is minimized. Each contact region is relatively small comparing to the size of the elastic object. There can be

This work was supported in part by the U.S. National Science Foundation under Grant IIS-0328782 and the National Basic Research Development Program of China (973 Program) (No. 2002CB312102), the National Natural Science Foundation of China (No. 60775057, No.60675047), the National High Technology Research and Development Program of China (863Program) (No. 2006AA04Z246, No. 2006AA01Z329) and 2007 Graduate Science and Technology Innovation Plan of Jiangsu Province (No. CX07B_075Z).

Tong Cui and Aiguo Song are with School of Instrument Science and Engineering, Southeast University, Nanjing 210096, P.R.China.

Jing Xiao is with the IMI Lab, Department of Computer Science, University of North Carolina – Charlotte, Charlotte, NC 28223, USA. E-mail: xiao@uncc.edu.

This work was done when Tong Cui was a visiting scholar at the above lab.

multiple contact regions between the rigid object and the elastic object at the same time, but multiple contact regions are formed one by one. This last assumption is reasonable since "simultaneous" contacts can be modeled as contacts that occur at instants very close to one another.

B. Building a Beam-Skeleton

Once a contact region is formed, a nonlinear model is used to simulate contact force exerted to the held rigid object by the elastic object from the contact region. Next, a beam-skeleton is built (see Fig.1), where between the (equivalent) contact point and an anchor point, a beam is established. The force **F** applied to the contact or equivalent contact point from the rigid object to the elastic object can be obtained as opposing the contact force response from the elastic object with the same magnitude. It can be viewed as applied to the common end of all the beams in the skeleton as the sum of the forces $\mathbf{F}^i$ applied to each beam at the common end. The distribution of **F** to $\mathbf{F}^i$ and the deformation of each beam *i* can then be computed based on the Bernoulli–Euler bending beam theory. After the stresses and strains at each beam end (i.e., each anchor point) are computed, the corresponding deformation displacement can be obtained. The deformation displacements over the entire surface are obtained via smooth interpolation of the values at anchor points to simulate global shape deformation of the elastic object [10].

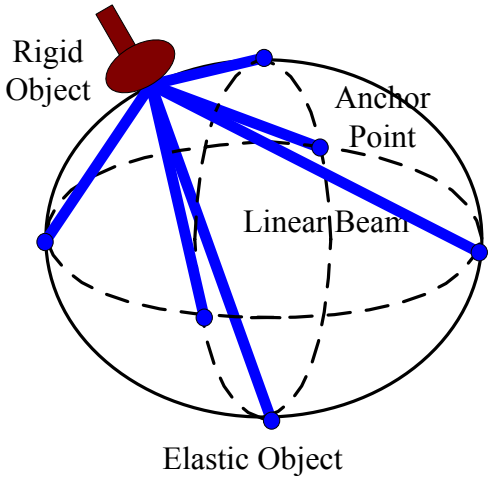

Fig. 1 A beam-skeleton

C. Multiple Contact Regions

Since multiple contact regions occur one by one in a temporal order, their combined effects on an anchor point can be computed accordingly in the same order. As a beam skeleton is established for each contact region one by one, for any anchor point of the elastic object, we can see multiple beams from multiple contact regions occur one by one, and each beam is connected to the position of the anchor point as the result of accumulated deformations from beams established previously.

As contact regions happen one by one, each intermediate shape deformation of the elastic object corresponding to the already happened contacts is obtained one by one, and the final deformed shape is the result of all contact regions [10].

III. Extending the Beam-Skeleton Model

The original beam-skeleton model requires that the elastic object be convex when undeformed, so that between a contact or equivalent contact point and an anchor point, there is always a straight-line connection inside or on the elastic object. Thus, a straight-line beam can be used.

If the elastic object has holes and is thus non-convex, there may not be a straight-line connecting the contact or equivalent contact point and an anchor point. In the latter case, a straight-line beam as introduced in [10] cannot work.

We focus in this paper deformation modeling of elastic objects with convex and smooth outer shapes and a hole inside by extending the beam-skeleton model to include circular cantilever beams. Fig. 2 shows a few such objects.

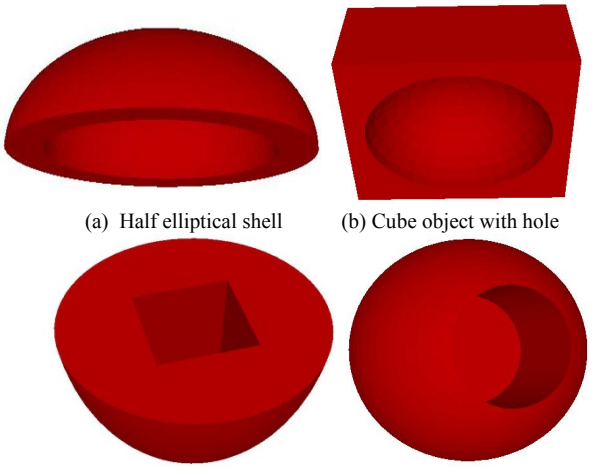

(a) Half elliptical shell (b) Cube object with hole

(c) Parabolic object with hole (d) Spherical object with hole

Fig. 2 Some elastic objects with holes inside.

A. Force Analysis based on Curved Beam Theory

Consider a circular cantilever beam with one end fixed and the other end bent. The beam is characterized by the following parameters: the angle Θ between the two ends of the beam and the inner and outer radii *a* and *b* of the beam. Establish the beam polar coordinate system as $O - r\theta$ frame, as shown in Fig. 3. Once the beam is pressed at the end that is not fixed, the exerted force effect is generally the combination of a radial component F_1 and a tangential component F_2. The total force generated on the beam is the vector sum of the radial force and tangential force.

According to the Curved Beam Theory [11-12], for any point with coordinates (r,θ) on the beam as shown in Fig. 3, we can relate F_1 to the radial stress σ_{r1} and tangential stress $\sigma_{\theta 1}$ on that area as follows.

$$\sigma_{r_1} = \frac{F_1}{N}\left(r - \frac{a^2+b^2}{r} + \frac{a^2b^2}{r^3}\right)\sin\theta$$

$$\sigma_{\theta_1} = \frac{F_1}{N}\left(3r - \frac{a^2+b^2}{r} - \frac{a^2b^2}{r^3}\right)\sin\theta$$

$$N = a^2 - b^2 + (a^2+b^2)ln\frac{b}{a}$$

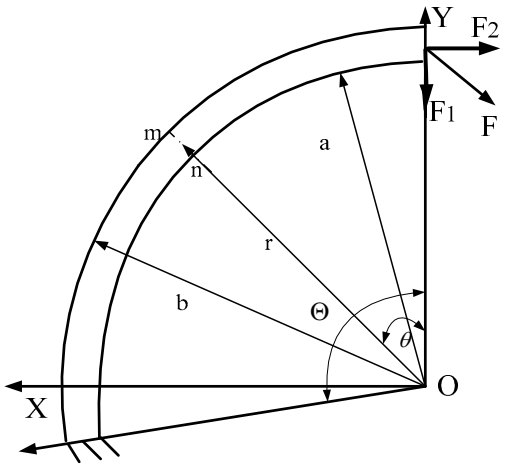

Fig. 3 A circular cantilever beam and the exerted force in polar coordinates

Similarly, we can relate F_2 to the radial and tangential stresses as follows.

$$\sigma_{r_2} = \frac{F_2}{N}\left(-r + \frac{a^2+b^2}{r} - \frac{a^2b^2}{r^3}\right)\cos\theta$$
$$\sigma_{\theta_2} = \frac{F_2}{N}\left(-3r + \frac{a^2+b^2}{r} + \frac{a^2b^2}{r^3}\right)\cos\theta$$

B. Circular Beam Deformation

We now describe how to compute the radial strain ε_r and the tangential strain ε_θ from the stresses of a circular beam and subsequently compute the deformation of the circular beam.

Define

$$A_j = \frac{1}{2N}F_j$$
$$B_j = -\frac{a^2b^2}{2N}F_j$$
$$D_j = -\frac{a^2+b^2}{N}F_j \quad (j = 1,2) \quad (1)$$

E is the Young's modulus, and μ is Poisson's ratio.

For the exerted force F_1, the relation between the strain ε_{r1} at a point and the two stresses σ_{r1} and $\sigma_{\theta 1}$ can be represented using the Hooke Generalized Theorem as:

$$\varepsilon_{r1} = \frac{1}{E}(\sigma_{r1} - \mu\sigma_{\theta 1}) = \frac{\sin\theta}{E}\left[2(1-3\mu)rA_1 - \frac{2(1+\mu)B_1}{r^3} + \frac{D_1}{r(1-\mu)}\right]$$

The tangential strain $\varepsilon_{\theta 1}$ can be expressed as:

$$\varepsilon_{\theta 1} = \frac{1}{E}(\sigma_{\theta 1} - \mu\sigma_{r1}) = \frac{\sin\theta}{E}[2(3-\mu)rA_1 + \frac{2(1+\mu)B_1}{r^3} + \frac{(1-\mu)D_1}{r}]$$

Similarly, for the exerted force F_2, the relation between the strain ε_{r2} and $\varepsilon_{\theta 2}$ at a point and the two stresses σ_{r2} and $\sigma_{\theta 2}$ can be shown as following:

$$\varepsilon_{r2} = \frac{1}{E}(\sigma_{r2} - \mu\sigma_{\theta 2}) = \frac{\cos\theta}{E}\left[2(1-3\mu)rA_2 - \frac{2(1+\mu)B_2}{r^3} + \frac{(1-\mu)D_2}{r}\right]$$

$$\varepsilon_{\theta 2} = \frac{1}{E}(\sigma_{\theta 2} - \mu\sigma_{r2}) = \frac{\cos\theta}{E}[2(3-\mu)rA_2 + \frac{2(1+\mu)B_2}{r^3} + \frac{(1-\mu)D_2}{r}]$$

The relation between the strain $[\varepsilon_r, \varepsilon_\theta]^T$ and the deformation displacement $[u, v]^T$ at the point can be represented as

$$\epsilon = \begin{bmatrix}\epsilon_r \\ \epsilon_\theta\end{bmatrix} = \begin{bmatrix}\frac{\partial}{\partial r} & 0 \\ 0 & \frac{\partial}{\partial\theta}\end{bmatrix}\begin{bmatrix}u \\ v\end{bmatrix}$$

The radial displacement $[u_1, v_1]$ and the tangential displacement $[u_2, v_2]$ of any point on a circular beam, caused by F_1 and F_2, respectively, can be expressed as [13-14]:

$$u_1 = -\frac{2\theta\cos\theta}{E}D_1 + K_1\sin\theta + L_1\cos\theta + \frac{\sin\theta}{E}[(1-3\mu)r^2A_1 + (1+\mu)r^{-2}B_1 + (1-\mu)lnrD_1] \quad (2)$$

$$u_2 = \frac{2\theta\sin\theta}{E}D_2 + K_2\sin\theta + L_2\cos\theta + \frac{\cos\theta}{E}[(1-3\mu)r^2A_2 + (1+\mu)r^{-2}B_2 + (1-\mu)lnrD_2] \quad (3)$$

$$v_1 = \frac{2\theta\sin\theta}{E}D_1 + K_1\cos\theta - L_1\sin\theta + H_1r + \frac{\cos\theta(1+\mu)}{E}D_1 - \frac{\cos\theta}{E}[(5+\mu)r^2A_1 + (1+\mu)r^{-2}B_1 - (1-\mu)lnrD_1] \quad (4)$$

$$v_2 = \frac{2\theta\cos\theta}{E}D_2 + K_2\cos\theta - L_2\sin\theta + H_2r - \frac{\sin\theta(1+\mu)}{E}D_2 + \frac{\sin\theta}{E}[(5+\mu)r^2A_2 + (1+\mu)r^{-2}B_2 - (1-\mu)lnrD_2] \quad (5)$$

where K_1, K_2, L_1, L_2, H_1, H_2 are displacement parameters, which can be expressed as functions of a, b, Θ, μ, E, A_j, B_j, and D_j (j = 1, 2).

So the new position of a point on the beam (after bending) can be obtained from the computed displacement. The total deformation at a point of a beam is the vector sum $[u_1+u_2, v_1+v_2]$.

C. Beam Selection Rules

We consider beams of constant width w=b-a, where w is determined as much smaller than the minimum thickness of the elastic object between its outer surface and the hole surface.

Given a contact or equivalent contact point P and an anchor point A on the surface of the elastic object, we first use the plane determined by the two points and the contact force **F** on P to intersect with the elastic object to obtain a

cross section of the elastic object[1]. Note that P and A are on the outer boundary of the cross section S; N_p and N_a are the normal vectors on the two points in the cross section respectively. Denote the curve between points P and A on the cross section S as Γ. Since the elastic object has a convex outer surface, Γ is convex (as shown in Fig. 4). Let ρ_{min} be the smaller curvature at either point P or point A. We can determine the outer radius b of a circular beam connecting P and A as $b = (1/|\rho_{min}|) + \varepsilon$, where $\varepsilon > 0$ can be as small as desired. From the outer radius and the two points P and A, the center C of the circular beam can be found. Since ε can be made arbitrarily small, the circular beam found above can be made as close to Γ as possible and inside S.

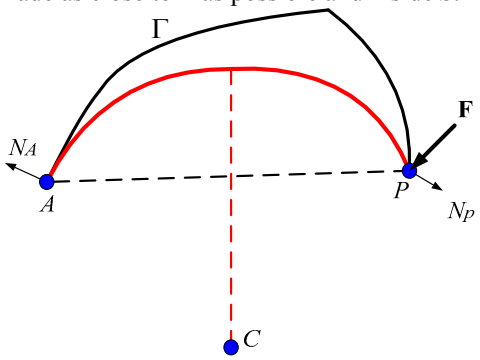

Fig. 4 A circular beam

Fig. 5 shows an example object and its beam-skeleton built corresponding to a contact point P. It consists of circular cantilever beams connected to different outer and inner anchor points of the object surface, and different circular beams may have different centers in polar coordinates.

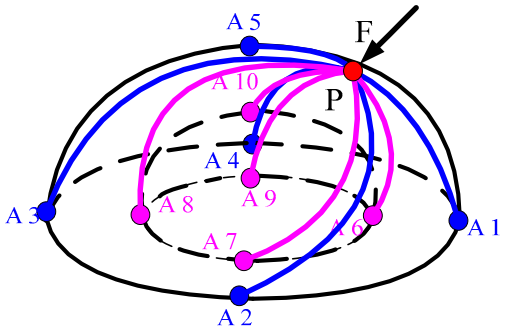

Fig. 5 A beam skeleton of circular beams for an elastic half elliptical shell

D. Contact Force Distribution to Circular Beams

Next we analyze how to distribute the total contact force $\mathbf{F}$ to each of the circular beams in a beam skeleton. Let $\mathbf{F^i}$ be the force distributed to the i-th beam. Let $\mathbf{F_1^i}$ and $\mathbf{F_2^i}$ be the radial and the tangential components of $\mathbf{F^i}$.

Let d^i be the distance between the contact point P and the center point C^i of the i-th circular beam. Represent the total deformation depth at the contact point P in the polar coordinate system of the i-th beam as $u_p^i + v_p^i$. According to equations (2)-(5), we can obtain:

$$u_p^i = u_{p_1}^i|_{\theta^i=0} + u_{p_2}^i|_{\theta^i=0} = L_1^i + L_2^i + \frac{\left[A_2^i(1-3\mu)\,d^{i\,2} + B_2^i(1+\mu)\,d^{i^{-2}} + D_2^i(1-\mu)ln\,d^i\right]}{E} = \varphi_u^i(F_1^i, F_2^i)$$

$$v_p^i = v_{p_1}^i|_{\theta=0} + v_{p_2}^i|_{\theta=0} = K_1^i + K_2^i + (H_1^i + H_2^i)\,d^i - \frac{A_1^i(5+\mu)\,d^{i\,2} + B_1^i(1+\mu)\,d^{i^{-2}} - D_1^i(1+\mu)}{\mathrm{E}} + \frac{D_1^i(1-\mu)ln\,d^i}{\mathrm{E}} = \varphi_v^i(F_1^i, F_2^i)$$

So u_p^i and v_p^i are both functions related to $\mathbf{F_1^i}, \mathbf{F_2^i}$, from which we can express $\mathbf{F_1^i}, \mathbf{F_2^i}$ as function of the known u_p^i and v_p^i, which are easy to derive.

$$F_1^i = \omega_1^i(u_p^i, v_p^i)$$
$$F_2^i = \omega_2^i(u_p^i, v_p^i)$$

For n circular beams, we can use the above to obtain the distribution of force $\mathbf{F}$ to the n beams:

$$F_1^1 : \cdots : F_1^i : \cdots : F_1^n = \omega_1^1(u_p^i, v_p^i) : \cdots : \omega_1^i(u_p^i, v_p^i) : \cdots : \omega_1^n(u_p^i, v_p^i)$$

$$F_2^1 : \cdots : F_2^i : \cdots : F_2^n = \omega_2^1(u_p^i, v_p^i) : \cdots : \omega_2^i(u_p^i, v_p^i) : \cdots : \omega_2^n(u_p^i, v_p^i)$$

Additionally, the vector sum of all $\mathbf{F^i}$'s, represented back in the world coordinate system, equals to $\mathbf{F}$.

E. Global Shape Deformation

With the method described in Section III.A and B, the deformation of a point on a circular beam can be computed. Now imagine the fixed end of the beam, i.e., at the anchor point, is no longer fixed, in which case, the stress will make it move to a new position. The position change can be considered as the deformation from the stress, which can be computed, again, as described in Section III.B.

With the deformation displacements of all beam ends of the elastic object and that of the contact (or equivalent contact) point obtained, the globally deformed shape of the entire elastic object can be obtained by interpolation, as described in [10].

IV. Implementation and Experimental Results

We tested our method in a virtual environment with real-time haptic rendering involving a virtual rigid body connected to a PHANToM Premium 1.5/6-DOF device, which moves the virtual rigid body to contact an elastic object with a hole. The haptic device is connected to a PC with dual Intel Xeon 2.4 GHz Processors and 1 GB system RAM. The bottom center of the elastic object is fixed, where a world coordinate system is set. We have tested our

[1] We only consider the case where $\mathbf{F}$ is not parallel to the line connecting P and A.

program by making our rigid object to contact some virtual rubber objects of different shapes and with holes.

Fig. 6 shows the flow chart of our program, where each iteration indicates one time-step "update" of contact force and resulting shape deformation. The work presented in this paper is highlighted in bold.

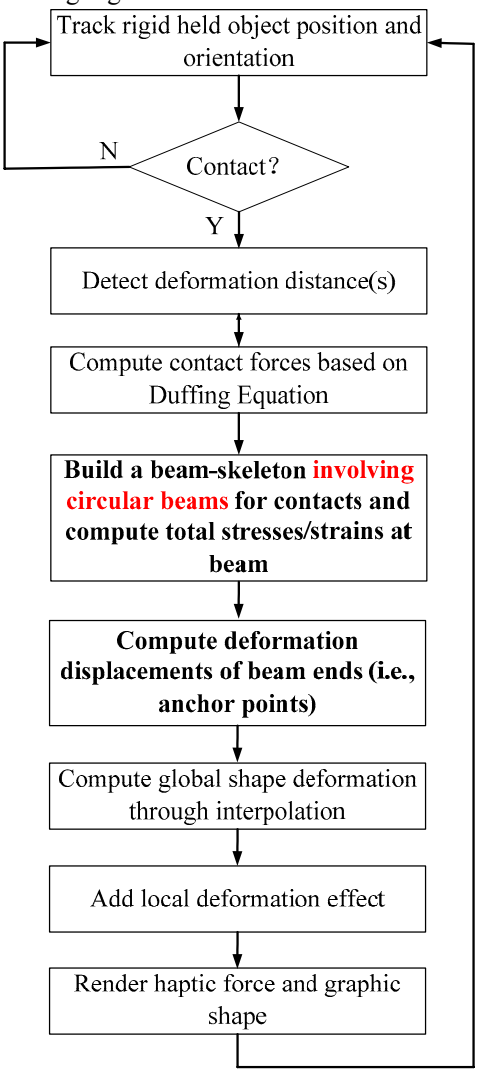

Fig. 6 Program flowchart

Within a small neighborhood of each separate contact region, the deformation at each point is actually a logarithmic function with respect to the distance to the contact region [15]. Thus, the global shape deformation (as the result of linear interpolation of deformations at anchor points) is modified [10] to reflect this non-linear property.

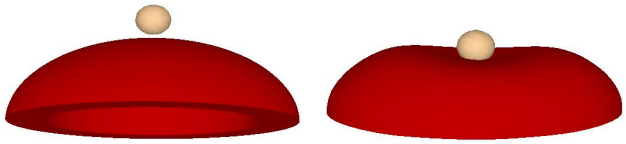

(a) (b)

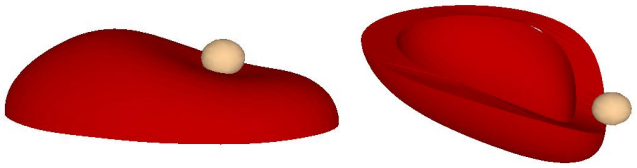

(c) (d)

Fig.7 Shape deformation of an elastic, half elliptical shell

Fig. 7 shows the deformation results modeled by our method of a half elliptical shell made of rubber, whose anchor points are shown in Fig. 5.

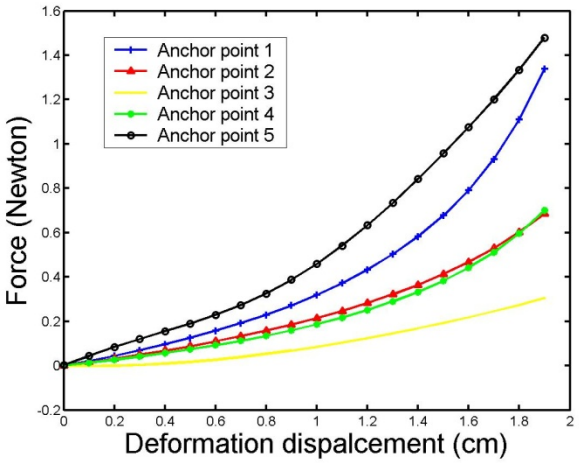

Fig. 8 Comparing force at different outer anchor points in Fig.7 (c)

Fig. 8 shows the result of comparing forces at each of the 5 anchor points on the outer boundary of the half elliptical shell in Figure 7 (c). Results on the 5 inner anchor points are similar. The force at each anchor point starts from zero and increases as the rigid object presses harder and the deformation deepens. Its magnitude is the result of the deformation of the corresponding circular beam under the contact force distributed to that beam. Anchor points closer to the contact point are under greater forces, which is reasonable.

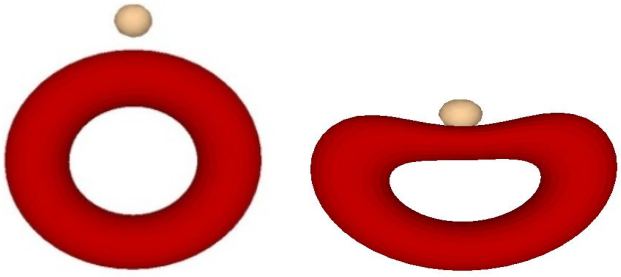

Fig.9 A rubber ring and the resulted shape deformation

Fig. 9 shows the deformation of a rubber ring object and the results of shape deformation modeled by our method.

For the grasping example shown in Figure 10, we use different keys on a keyboard to interactively control different fingers or different joints on a finger of a virtual hand to achieve a grasp of the virtual elastic object [16]. In

the process, our algorithm provides real-time rendering of the changing shape of the elastic object and the time series of the contact forces.

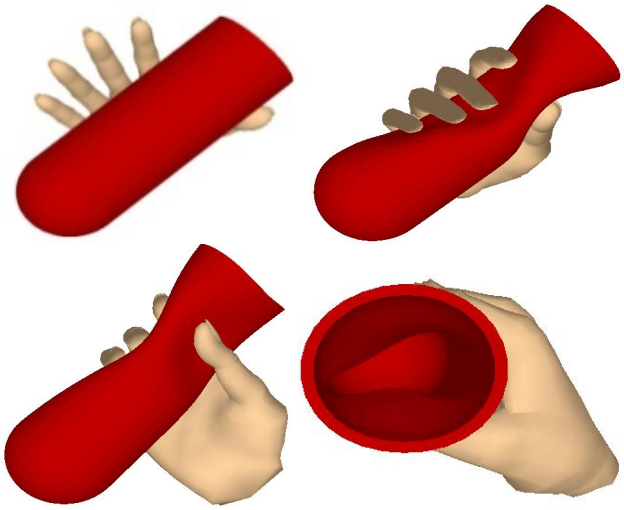

Fig. 10 Different grasps of an elastic cylindrical object with hole and the resulted shape deformation

In all of our experiments, modeling and computing haptic force per contact region took a constant and almost instant frequency in the order of k Hz, which satisfies the requirement for real-time simulation of contact force and shape deformation in haptics. In all the examples, the numbers of triangles in the mesh models of objects range from 2000 to 6000. Table 1 lists the parameters used in our experiments, where M is the weight of the elastic object, E is the Young's modulus, I is the moment of inertia, and μ is Poisson's ratio.

TABLE I
PARAMETERS OF ELASTIC OBJECT USED IN EXPERIMENTS

Parameter	Half ellipse	Ring	Cylinder
M(kg)	1.0	1.0	1.0
Mesh	5428	2304	3024
Thickness (mm)	10	20	10
$\varepsilon(mm)$	0.5	1	0.5
$I(kg/cm^2)$	100	100	100
$E(N/m^2)$	$3 \cdot 10^6$	$3 \cdot 10^6$	$3 \cdot 10^6$
μ	0.47	0.47	0.47

V. CONCLUSIONS

This paper extends the beam-skeleton method introduced in [10] by introducing circular beams to model the global shape deformation of an elastic object with an outer convex shape and a hole when a rigid object contacts it. The method strikes a good balance between simulation efficiency and physical realism. The results show the efficiency and effectiveness of the method. Future work includes investigating further extension into modeling global deformation of more general objects with non-convex outer shapes and with holes.

REFERENCES

[1] J. Shen, Y. H. Yang, "Deformable Object Modeling Using the Time-Dependent Finite Element Method," *Graphical Models and Image Processing*, November 1998, 60(6):461-487.

[2] F. Conti, O. Khatib, and C. Baur, "Interactive rendering of deformable objects based on a filling sphere modeling approach," in IEEE Int. Conf. Robotics and Automation, 2003, pp. 3716–3721.

[3] K. Sundaraj, C. Mendoza, C. Laugier, "A fast method to simulate virtual deformable objects with force feedback,"7th International Conference on Control, Automation, Robotics and Vision, 2002, pp. 413 – 418.

[4] L.P. Nedel and D. Thalmann, "Real time muscle deformations using mass-spring systems," *Computer Graphics International*, 1998, pp. 156–166.

[5] O. R. Astley and V. Hayward, "Multirate haptic simulation achieved by coupling finite element meshes through Norton equivalents," IEEE International Conference Robotics and Automation, May 1998, pp. 989–994.

[6] J. Berkley, G. Turkiyyah, D. Berg, M. Ganter, and S.Weghorst, "Realtime finite element modeling for surgery simulation: An application to virtual suturing," *IEEE Trans. Vis. Comput. Graphics*, 2004, pp. 314–325.

[7] K. Hirota and T. Kaneko, "Haptic Representation of Elastic Objects?" MIT *Presence*, 2001, 10(5): 525-536.

[8] R. Balaniuk and K. Salisbury, "Soft-Tissue Simulation Using the Radial Elements Method," *Surgery Simulation and Soft Tissue Modeling*, v2673, 2003.

[9] M. Wicke, D. Steinemann, and M. Gross, "Efficient animation of point-sampled thin shells," *Computer Graphics Forum*, September 2005, 24(3): 667-676.

[10] Q. Luo and J. Xiao, "Contact and Deformation Modeling for Interactive Environments," *IEEE Transactions on Robotics*, 2007, 23(3): 416-430.

[11] A. I. LUR'E, *Theory of Elasticity*, Nauka, Moscow, 1970.

[12] N. M. Borodachev, "The equations of compatibility of deformations," *Journal of Applied Mathematics and Mechanics*, 2001, 65(6): 1021-1024.

[13] M. H. Sadd, *Elasticity - Theory, Applications and Numerics*, New York, 2005.

[14] I. V. Andrianov, J. Awrejcewicz, "Compatibility Equations in the Theory of Elasticity," *Journal of Vibration and Acoustics*, April 2003, 125(2): 244-245.

[15] Q. Luo and J. Xiao, "Geometric Properties of Contacts Involving a Deformable Object," IEEE Symposium on Haptic Interfaces for Virtual Environment and Teleoperator Systems, Washington D.C., March 25--26, 2006, pp. 533-538.

[16] T. Cui and J. Xiao, "Simulation of Grasping Deformable Objects with a Virtual Human Hand," IEEE/RSJ International Conference on Intelligent Robots and Systems, Nice, France, Sept. 2008. pp. 3965-3970.